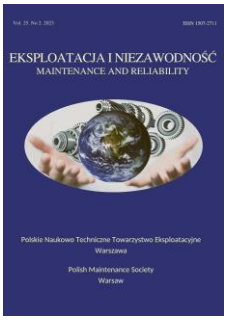

Eksploatacja i Niezawodnosc – Maintenance and Reliability
Volume 28 (2026), Issue 3
journal homepage: http://www.ein.org.pl

Article citation info:
Liu X, Dong Y, Li F, Wang Y, Zhao L, Wang J, Analysis of mechanical characteristics and structural optimization of continuous mining machine track based on two-way coupling, Eksploatacja i Niezawodnosc – Maintenance and Reliability 2026: 28(3) http://doi.org/10.17531/ein/218130

Analysis of mechanical characteristics and structural optimization of continuous mining machine track based on two-way coupling

Indexed by: Web of Science Group

Xunan Liu[a,b], Yongqiang Dong[a,*], Faquan Li[c], Yadong Wang[a], Lijuan Zhao[a,b], Jianyong Wang[d]

[a] School of Mechanical Engineering, Liaoning Technical University, China
[b] State Key Lab of mining machinery engineering of coal industry, China
[c] CCTEG Taiyuan Research Institute, China
[d] Ningxia Polytechnic, China

Highlights

- Coupled DEM-MFBD model reflects track system behavior under real conditions.
- Kriging-GA integration enables efficient optimization.
- Parametric modeling is used for structural optimization.
- Calculate the force during the process of the drum cutting coal and rock.

Abstract

During the cutting process of continuous miners, track plates are prone to deformation and damage, adversely affecting operational reliability and production efficiency. This study focuses on the EML340 continuous miner and establishes a simulation model based on the Discrete Element Method–Multi-Flexible Body Dynamics (DEM-MFBD) bidirectional coupling technology. Simulation results indicate that the load is mainly concentrated on the tight side of the track, with increasing intensity near the drive sprocket. The original track plate exhibits a maximum equivalent stress of 758.2 MPa and a safety factor of only 1.22. To address this issue, a multi-objective genetic algorithm implemented on the ISIGHT platform was employed to optimize the track plate structure, aiming to reduce weight and improve the safety factor. The optimized track plate weighs 25.42 kg, achieving a 9.2% reduction in weight compared to the original design, while the safety factor increases from 1.22 to 1.43. Industrial tests demonstrate that the optimized track plate operates without failure during service.

Keywords
DEM-MFBD, track plate, structural optimization, continuous mining machine, ISIGHT

1. Introduction

The continuous mining machine is mainly used in the room and pillar coal mining method and can also be employed for roadway excavation. It is suitable for 1.5 m - 6 m coal seam mining and is a large-scale continuous mining equipment integrating cutting, loading, and transporting. The traveling part of the continuous mining machine supports the weight of the entire machine and provides traction for the advancement and cutting of the entire machine. The structure of the traveling part is shown in Figure 1. During the propulsion and cutting of the continuous mining machine, the bearing capacity of the roadway floor and the force on the track plate at different positions are not the same. This phenomenon can be attributed to the non-equilibrium, non-linear, time-varying, and strong coupling nature of the drum-cutting coal rock load [1], as well as the unevenness of the roadway floor. This effect leads to the track plate being subjected to complex alternating loads with significant load fluctuations. The track plate is subjected to stresses such as extrusion and bending and is prone to fracture

(*) Corresponding author.
E-mail addresses: X. Liu (ORCID: 0000-0003-0737-2475) yuwuknan@163.com, Y. Dong (ORCID: 0009-0009-9687-4151) 2422034330@qq.com, F. Li, 18734827992@163.com, Y. Wang, 1135514607@qq.com, L. Zhao, zzz2120@126.com, J. Wang, nxcrc@163.com

and deformation. Figure 2 illustrates the failure condition of the track of a certain machine model, such failure increases the downtime for equipment maintenance. Frequent replacement and repair of the track plates increase the operating costs and affect the production efficiency of the coal mine. Therefore, researchers have conducted extensive investigations on the failure mechanism from the perspectives of theoretical analysis, multi-flexible body dynamics, and structural optimization.

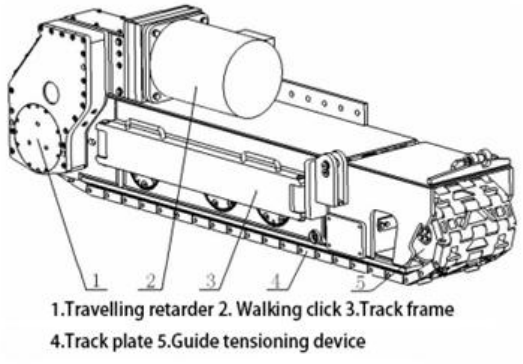

Figure 1. Simple structure diagram of the track walking part.

Figure 2. Track plate damage.

In terms of theory and dynamic simulation. Initially, Bekker et al. [2] proposed the famous soil-bearing pressure-sinking relation equation based on the soil mechanics theory, improving the crawler. With the development of computer technology, more and more researchers are conducting analysis and research through virtual prototyping technology. In order to enhance the reliability of bauxite mining machines, Xu et al. [3] conducted rock crushing tests using servo presses and cutting test devices. The working process of the drum was simulated by using the finite element method, and the forces acting on the entire drum and each conical tooth were studied. Wan et al. [4] analyzed the dynamic response of the cutting equipment. The finite element method was adopted to establish the drum of the coal shearer. The relationship between the vibration characteristics of the drum of the coal shearer and the coal mining performance during the coal mining process was analyzed, which is conducive to improving the reliability of the coal shearer. Han et al. [5] explored the dynamic characteristics of the track travel system through dynamic simulation technology; the contact force between the track plate, the roadwheel, and the ground was analyzed, providing a reference for the contact force between the track plate and the driving wheel. Liu et al. [6] established a track system model using ADAMS multi-body dynamics simulation software and conducted an in-depth analysis of the dynamic response of the constructed model. Zhu and Gu et al. [7] established a finite element model of the track, carried out a strength calculation of the track, analyzed the distribution of stress and deformation of the track parts, and found the locations where the maximum stress and deformation of the parts occurred, providing a basis for the optimal design of the track plate. Lu et al. [8] introduced the composition structure and working principle of the caterpillar walking mechanism of a continuous mining machine. Furthermore, the authors analyzed the force of the caterpillar plate and pin, providing a theoretical basis for designing the caterpillar walking mechanism of a continuous mining machine. Zhang et al. [9] simulated the multi-flexible body dynamics of the crawler traveling mechanism of a certain continuous shearer based on the dynamics software RecurDyn. The authors obtained the load characteristic curve of the crawler traveling mechanism. Furthermore, they also analyzed the load contact characteristics and modal stress response characteristics of the engagement between the sprocket teeth and the crawler plate, provided a concrete solution to the fault identification of the continuous shearer track traveling mechanism. Shi et al. [10] used the traditional gear strength calculation formula and the finite element method to analyze the force of the driving wheel of the ML360 continuous shearer. Compared with the traditional method, the bending stress deviation of the gear calculated by the finite element method was 7%, verifying the accuracy of the finite element analysis method. Wei et al. [11] established the track-ground interaction system space via the computer simulation software and investigated the track traveling resistance with this system. Zhang et al. [12] established the multi-flexible body dynamics model of the continuous shearer track driving system based on RecurDyn. Furthermore, the authors obtained the stress at the root of the driving wheel and

the vibration acceleration at different positions of the vehicle body. The study on the dynamic load of the track driving system reduced the test cost. It provided a good theoretical basis for the reliability study of the track-driving system of coal mine machinery. Yang et al. [13] used the finite element analysis method to analyze the damage to the track plate in the track traveling mechanism. Zivkovic et al. [14] conducted a reliability assessment of the instantaneous failure rate, estimated failure rate and assigned failure rate of planetary transmission and its components using a "bottom-up" approach. The above research provided the basis for studying the dynamic characteristics of the track. In terms of optimization. Gao et al. [15] utilized the genetic algorithm (GA) to optimize the parameters of the Kriging model and combined it with the distributed collaborative strategy, introducing the distributed collaborative Kriging model optimized by the genetic algorithm (DCGAK). This method enriches the existing methods for structural reliability analysis of complex mechanical systems. Lao et al. [16] proposed a collaborative optimization method based on the improved NSGA-II algorithm to enhance the efficiency and reliability of the drum. Firstly, the influence of spiral blades on the coal conveying performance was analyzed by using the Discrete Element Method (DEM), and the new designs of two types of coal guiding rollers were studied. Subsequently, an NSGA-II enhancement strategy based on spatial density was proposed to collaboratively optimize the drum body structure and motion parameters. Ling et al. [17] conducted a multi-objective optimization design for the EBZ-135 tracked roadheader to enhance the adhesion and silt removal of the track plate by referring to the design of the tank track. Lastly, the authors verified the feasibility of the optimization via ADAMS. Zhang et al. [18] adopted fuzzy control and genetic algorithms to optimize the control strategy of the chassis electric drive system and solve the cooperative control problem of the dual motor system of the excavator track driving mechanism. Good excavator driving performance and control effect were achieved after optimization. Fei and Li et al. [19] employed the optimization theory to establish an optimization model aiming at maximum adhesion solved by the genetic algorithm. The authors wanted to explore the weakness of the roadheader's poor walking ability on the sparse, soft roadway floor. Qin et al. [20] established a response surface model of the track plate with the mass and minimum equivalent stress of the track plate as the optimization objectives. Moreover, the authors employed a genetic algorithm to solve the response surface model, providing a theoretical basis and engineering design guidance for track plate bonding optimization. Si et al. [21] optimized and improved the structure of the walking track plate of the existing EBZ160 roadheader in Sihe Coal Mine according to its defects, adding several grounding tendons, the results were compared based on ADAMS software, showing a good optimization effect. The proposed model can discharge the mud adhering to the structure of the track plate, avoiding the skidding phenomenon caused by excessive mud adhesion. Zheng and Wang et al. [22] calculated the maximum wheel pressure of the supporting wheel of the crawler crane and the wheel-plate contact stress under the over-lifting working condition through theoretical methods. Then, the authors conducted a contact analysis of the wheel-plate structure using finite element simulation software. Finally, they performed the lightweight design of the supporting wheel using the MOGA multi-objective genetic algorithm.

Many researchers have conducted studies on tracks from different perspectives. In terms of dynamics simulation, in most studies, the roadway floor model is simplified as a whole rigid flat plate, disregarding factors such as the inhomogeneity and deformation of the roadway floor. EDEM can finely characterize ground models and accurately simulate the physical behavior of granular substrates. However, it is limited by being unable to address complex dynamic problems. This paper establishes a two-way coupling model of continuous mining machine dynamics based on EDEM-RecuDyn, the dynamics analysis of the track of the continuous mining machine under the propulsion condition is conducted to obtain the real dynamics characteristics of the track during the working process. Most studies increase strength and stiffness to enhance the safety factor of the track structure by increasing the plate thickness or setting reinforcing ribs. However, this often increases the weight of the entire machine, affecting the mobility of the continuous mining machine. In this paper, a multi-objective genetic algorithm is employed to optimize the key structural parameters of the track plate based on the ISIGHT platform. The two-way coupled simulation data is taken as a sample to improve the track's safety factor and reduce the mass. Thus, the overall quality is lightweight to ensure the track's

safety, providing a new thought for the design, analysis, and optimization of the mining machinery structure, and it is of strong guiding significance.

2. The mechanical model

2.1. Measurement and verification of physical and mechanical parameters of roadway floor rock

The Zhangjiamao Coal Mine area is the working condition to make the constructed model closer to the actual situation. The roadway floor rock specimens' physical and mechanical parameters were tested per the testing standards, the related experiments are shown in Figure 3. The physical and mechanical parameters required for modeling the roadway floor and the bonding parameters of the roadway floor rock particles obtained from the literature [23] are shown in Table 1.

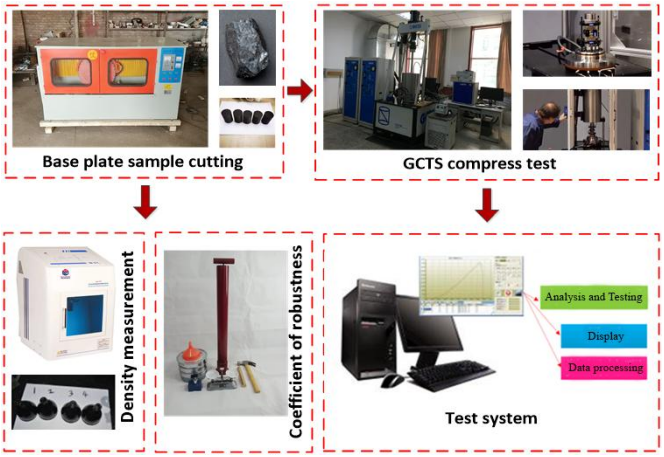

Figure 3. Floor rock sample performance test.

Table 1. Floor rock parameters.

Related genera	Floor rock
Density(ρ/(kg·m^{-3}))	2300
Poisson's ratio(μ)	0.31
Shear modulus(G/Pa)	1.50×10^{9}
Compressive strength(σ_1/Pa)	2.39×10^{7}
Coefficient of robustness	4
Normal stiffness per unit area(N/m^3)	2.9×10^{11}
Tangential stiffness per unit area(N/m^3)	1.5×10^{11}
Critical normal stress(Pa)	2.0×10^{7}
Critical tangential stress(Pa)	4.8×10^{7}

The GCTS(Rock mechanics Experimental System) is an experimental apparatus used to test the mechanical properties of rocks. It can simulate the stress state of rocks in situ and conduct various rock mechanics experiments. In these experiments, the failure modes of brittle materials, such as coal and rock, typically exhibited brittle fracture behavior, with rupture occurring along specific planes or paths, as shown in Figure 4. The experimentally obtained axial stress curve is shown in Figure 5(b), with the maximum axial stress reaching 23.9 MPa.

Figure 4. GCTS compression fracture.

A uniaxial compression test was simulated to ensure the feasibility of EDEM simulation of the floor. A 1:1 reproduction is not feasible due to the complexity of the particles in the floor of the underground roadway, hence, it is assumed that the particle sizes in the roadway are uniformly distributed. Moreover, the particle size should be neither too large nor too small. If the particles are too large, the authenticity of the simulation results will be compromised. If they are too small, the computational difficulty will increase, potentially preventing the solution from being obtained. Considering these factors and reference 19, particles with a radius of 10 mm were selected. In the uniaxial compression test, the floor specimen is a cylinder with a diameter of 250 mm and a height of 500 mm, the specimen was filled using a static particle generation method. The particle radius was 10 mm, and the bonding radius was 12 mm, the bonding between particles was modeled using the bonding model, with parameters shown in Table 1.

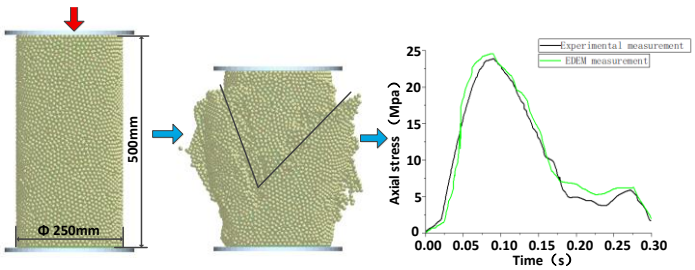

(a) Uniaxial compression model (b) Axial stress curve

Figure 5. Simulation experiment of uniaxial compression.

The model is depicted in Figure 5(a), an axial force was applied to the upper side of the cylindrical specimen until it fractured. The axial stress curve obtained in the post-processing is shown in Figure 5(b), the uniaxial compression test results agree with the EDEM simulation results. The maximum axial stress in the EDEM simulation was 24.4 MPa, i.e., relatively

close to the compressive strength listed in Table 1. Therefore, the feasibility of the discrete element model of the floor was validated, There are also literature studies on the interaction between vehicles and the ground, further verifying the feasibility of the particle discrete element method [24].

2.2. Calculation of cut-off roller loads

The cutting section of the continuous miner comprises three drums: left, center, and right, which are symmetrically distributed about the centroid of the center drum [25], as shown in Figure 6. For ease of description, the force analysis is presented as a simplified force diagram of the drum.

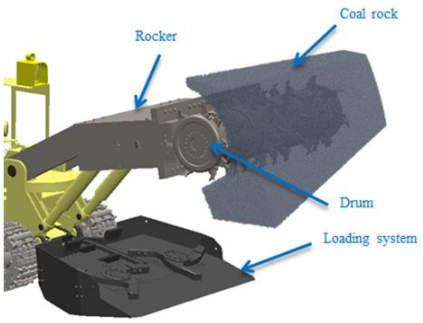

Figure 6. Cutting drum model diagram.

The forces in the axial direction are equal in magnitude but opposite in sign. Hence, they mutually counteract, rendering the axial force X_{ij} negligible. Figure 7 constitutes a force-cutting schematic of the drum of the continuous mining machine, the rotational speed of the drum is ω_b, the cutting teeth in contact with the coal are subjected to the cutting resistance Z_{ij} and the traction resistance Y_{ij}.

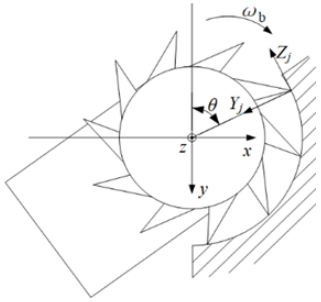

Figure 7. Shear force diagram.

1) Calculating the cutting and traction resistance of cutting teeth

$$Z_{ij} = 10\overline{A_p}\frac{0.35b_p+0.3}{b_p+K_\psi(h_{max}\sin\theta_{ij})^{0.5}}h_{max}\sin\theta_{ij}\cdot t_{cp}K_zK_yK_\psi K_cK_{ot}\frac{1}{\cos\beta} \quad (1)$$

$$Y_{ij} = (0.5\sim0.8)Z_{ij} \quad (2)$$

where Z_{ij} represents the cutting resistance of the jth tooth of the ith cutting line, N; Y_{ij} denotes the traction resistance of the jth tooth of the ith cutting line, N; $\overline{A_p}$ signifies the average cutting impedance of the non-ground-pressure-influenced area of the coal seam, N/mm; b_p indicates the calculated width of the working part of the cutting tooth, cm; h_{max} designates the maximum cutting thickness of the cutting tooth, cm; t_{cp} refers to the cutting width of the cutting tooth; K_z stands for the coefficient of the exposed free surface; K_y represents the influence coefficient of the cutting angle; K_φ indicates the influence coefficient of the shape of the rake face of the cutting tooth; K_c denotes the coefficient of the cutting tooth arrangement; K_{ot} symbolizes the influence coefficient of the ground pressure on the coal wall of the working face; β represents the deflection angle of the cutting tooth for the direction of traction or swinging, °; K_ψ indicates the brittleness coefficient of the coal; f′ refers to the cutting impedance coefficient; and θ_j represents the angle of the position where the jth cutting tooth is located, °.

2) Force analysis and transformation of cutting teeth

The cutting teeth' cutting resistance and traction resistance are decomposed into X and Y and then transferred to the center of mass. As depicted in Fig. 8, the magnitudes of the resultant forces of all cutting teeth X and Y are R_X and R_Y:

$$R_x = \sum_{i=1}^{N}R_{xi} = \sum_{i=1}^{N}\sum_{i=1}^{N}\left(-Z_{ij}\,sin\,\theta_{ij} + Y_{ij}\,cos\,\theta_{ij}\right) \quad (3)$$

$$R_y = \sum_{i=1}^{N}R_{yi} = \sum_{i=1}^{N}\sum_{i=1}^{N}\left(-Z_{ij}\,cos\,\theta_{ij} - Y_{ij}\,sin\,\theta_{ij}\right) \quad (4)$$

where N represents the total number of cutting lines; R_{xi} is the resultant force in the X direction on the cutting line where the cutting tooth is situated, N; R_{yi} is the resultant force in the Y direction on the cutting line where the cutting tooth is situated, N.

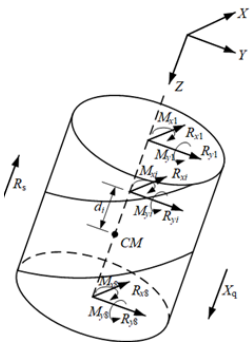

Figure 8. Shear force diagram.

The combined force is transferred to the center of mass of the drum while generating moments M_x, My, and M_z.

$$M_x = \sum_{i=1}^{N} R_{yi} \cdot d_i, \quad (5)$$

$$M_y = -\sum_{i=1}^{N} R_{xi} \cdot d_i, \quad (6)$$

$$M_z = \sum_{i=1}^{N} \sum_{j}^{n} Z_{ij} D \cdot 500, \quad (7)$$

where α represents the friction angle, °; d_i is the distance of the ith cutting line from the center of mass, mm; n represents the total quantity of cutting teeth on any cutting line; N represents the total number of cutting lines.

Based on the load calculation formula developed by the aforementioned research group [26], the load simulation program of the continuous mining machine was compiled based on MATLAB (version R2023b) software, the program flowchart is presented in Figure 9. The propulsion speed is set at 3.5 m/min, the rotational speed of the spiral drum at 51 r/min, the cutting depth at 330 mm, and the coal firmness coefficient at 3 [27]. The calculated three-directional force curves of the drum of the continuous mining machine are employed as the external loads of the drum rigid-flexible coupling model, as depicted in Figure 10.

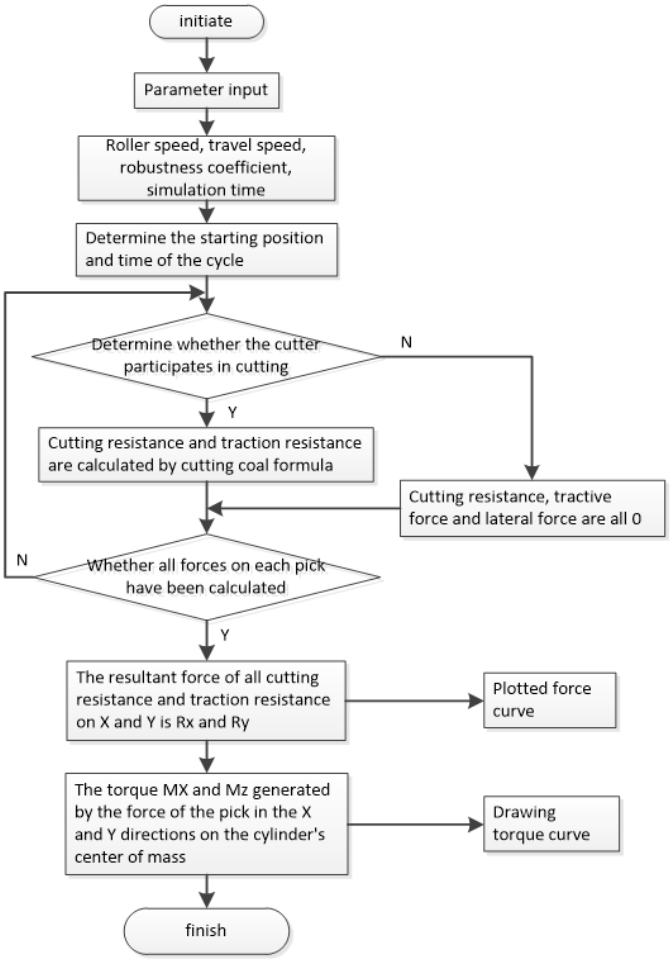

Figure 9. Flow chart of load calculation.

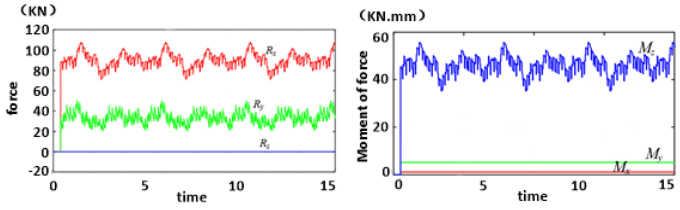

(a) Three-way force (b) three-way moment

Figure 10. Three-way force curve of drum cutting.

3) Hertz contact theory

The calculation of contact forces in RecurDyn is based on the modified Hertz contact theory to simulate real contact conditions more accurately. These modifications include stiffness coefficients, damping coefficients, and other relevant exponents to accommodate different contact characteristics. The contact force f_n between adjacent rigid bodies is calculated using the following formula:

$$f_n = K\delta^{m1} + C\frac{\dot{\delta}}{|\dot{\delta}|}|\dot{\delta}|^{m_2}\dot{\delta}^{m_3} \quad (8)$$

where:

δ is the mutual interference depth between the two objects, in mm;

$\dot{\delta}$ is the derivative of the contact penetration depth;

K is the contact stiffness coefficient;

C is contact damping;

m_1 is the contact stiffness index;

m_2 is the contact damping index (both m_1 and m_2 can produce nonlinear contact forces);

m_3 is the compensation index (dent index), i.e., a compensation damping effect is generated to avoid contact forces less than zero.

The calculation formula for k is:

$$k = \sqrt{\frac{16RE^2}{9}} \quad (9)$$

$$R = \frac{R_1 R_2}{R_1 + R_2} \quad (10)$$

$$E = \frac{E_1 E_2}{E_2(1-\gamma_1^2) + E_1(1-\gamma_2^2)} \quad (11)$$

where:

R_1 and R_2 are the contact radius of the corresponding entity, mm;

E_1 and E_2 are the elastic moduli of the corresponding entities, MPa;

γ_1^2 and γ_2^2 are the poisson's ratios of the corresponding

entities, respectively.

3. Construction of DEM-MFBD two-way coupling model

3.1. Establishing the dynamic model of the continuous mining machine based on RecurDyn

The continuous miner is primarily composed of the cutting unit, gathering arm unit, traveling unit, and hydraulic system, among other components. The dynamic loads generated during its cutting and advancing process are transmitted along the path "drum – cutting arm and hydraulic support – main frame – crawler system" and ultimately act on the crawlers. To accurately simulate this complete load transmission path and dynamic feedback mechanism, and to ensure the correctness of load application points, direction, and stress distribution, a detailed full-machine dynamic model was developed in this study. First of all, the models of each component of the continuous mining machine are constructed in SOLIDWORKS, and the assembly and interference are inspected to ensure there is no interference. The entire machine model of the continuous mining machine is imported into the dynamics simulation software RecurDyn in the x-t format. The material properties are assigned in accordance with the parameters in Table 2.

According to reference 23 [28], the contact parameters between the components in Table 3 are listed. In RecurDyn, the contact between the track plate, drive sprocket, and track frame was established via the Geo Contact method.

Table 2. Material parameters of each part of the walking part.

Material parameter	Track plate	Driving wheel	Track frame	Tensioning pulley
Density(kg·m^{-3})	7800	7800	7800	7800
Poisson's ratio(μ)	0.28	0.3	0.3	0.3
Shear modulus(G/Pa)	7.8×10^{10}	8×10^{10}	7.2×10^{10}	7.4×10^{10}

Table 3. Material parameters of each part of the walking part.

Contact parameter	Driving wheel Track plate	Tensioning pulley Track plate	Track frame Track plate
Stiffness (N/mm)	100000	100000	100000
Damping (N·S/mm)	1000	1000	900
Coefficient of dynamic friction	0.15	0.15	0.25
Stiffness index	1.5	1.5	1.5

Constraints are imposed between the components of the traveling part, and a drive is incorporated at the drive wheel. The theoretical speed of the continuous mining machine during the advancement and cutting operation is v_m = 3.5 m/min, with l_k = 0.14 m, Z_k = 5. Hence, the rotational speed of the drive wheel can be calculated as 5 r/min (30 °/s), the step function is selected to configure the drive: step (time, 1, 0D, 1, -30D).

$$v_m = \frac{z_k l_k}{2\pi} w_k = \frac{z_k l_k n_k}{60} \tag{12}$$

where v_m denotes the winding speed of the track (m/s), Z_k represents the effective number of meshing teeth of the drive wheel (number), l_k indicates the track pitch (m), w_k designates the angular speed of the drive wheel (rad/min), and n_k represents the rotational speed of the drive wheel (r/min).

As depicted in Figure 11, the track plates are sequentially numbered in the counterclockwise direction for the analysis. The track plates at specific positions 1, 5, 9, 13, 17, 21, 27, 31, 35, 39, 43, and 47 are flexibly processed to ensure the ergodicity of the stress and strain analysis of the track plate and reduce the simulation time without influencing the simulation results. The mesh adopts solid4, with a size range of 1 mm - 5 mm.

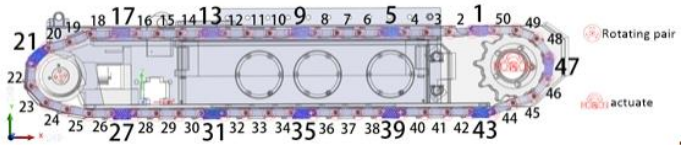

Figure 11. Track plate label and flexible processing.

The three-way force and moment curves of the centroid of the cutting drum derived in chapter 1 are imported into RecurDyn via text, the three-way force and moment are imposed at the centroid of the cutting drum by utilizing the screw and rforce commands of the force module. Only the track in contact with the discrete element bottom plate is exported as a wall file to prepare for the two-way coupling, enhancing the simulation efficiency. Hence, the simulation speed is guaranteed without influencing the simulation accuracy. Therefore, the rigid-flexible coupling model of the continuous mining machine is accomplished, as depicted in Figure 12.

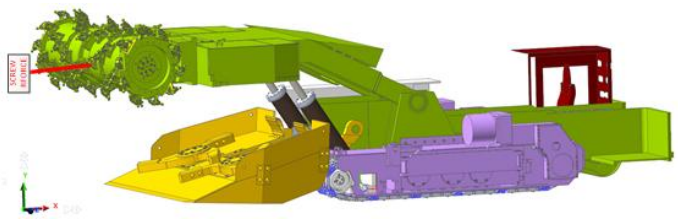

Figure 12. Rigid-flexible coupling model of continuous mining machine.

3.2. Construction of the roadway floor model based on EDEM

The discrete element floor model was constructed using the uniaxial compression simulation test. The roadway floor slab with a size of 9000 mm × 6000 mm × 200 mm is filled by using the static generation method, 800,000 particles were generated. The track wall file was imported into the roadway floor model, and the relevant material parameters were set, as shown in Figure 13.

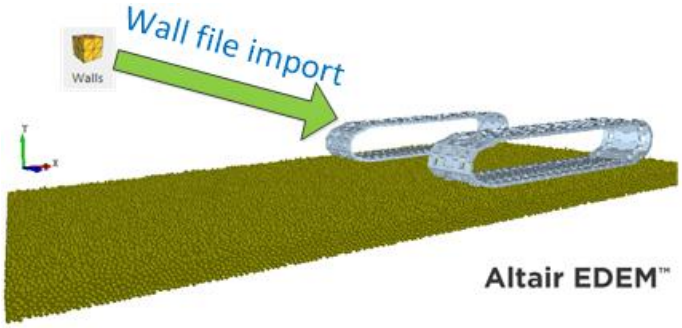

Figure 13. Discrete element ground model.

3.3. EDEM-RecurDyn two-way coupling space for the continuous mining machine

Due to the complex kinematic relationships, intricate loading conditions, and contact interactions between components within the entire track system, relying solely on the EDEM software for simulation is challenging. Reconstructing the complex dynamic constraints of the entire track system within EDEM would lead to a significant increase in modeling workload and a high probability of errors. More importantly, importing all moving parts into EDEM for processing would place an excessive burden on the solver, reducing computational efficiency by several times compared to the coupled approach, making it unsuitable for subsequent parametric studies and optimization. In contrast, the EDEM-RecurDyn coupling method employed in this paper fully leverages the core strengths of each specialized software (RecurDyn excels in multi-flexible body dynamics, while EDEM specializes in particle simulation). This approach ensures accuracy, particularly in capturing the flexible deformation of the track plates (MFBD), while achieving an optimal balance between modeling efficiency and computational cost. It enables the accurate analysis of the real-time state of the continuous miner's track during the cutting and propulsion process. The steps for the co-simulation are as follows:

(1) A dynamic model of the continuous miner was created in RecurDyn, the wall file of the track mechanism in contact with the discrete element ground was exported.

(2) A discrete element ground model was established in EDEM. The spatial coordinates and gravity direction are consistent with those in the dynamic model in RecurDyn to prevent simulation failure. The direction of the continuous miner's advance was defined as the X-axis and the direction of gravity as the Y-axis.

(3) The wall file was imported into EDEM. Only the track interacts directly with the discrete element ground during the cutting and advancing of the continuous miner, the remaining components have a relatively minor impact on the simulation results. Therefore, the bidirectional coupling model used only 100 track plates of the continuous miner. The coupling interface (start coupling server) was activated, and the co-simulation was initiated in RecurDyn.

(4) The target data were obtained using the post-processing modules of RecurDyn and EDEM.

In the bidirectional coupling calculation of DEM-MFBD, the time step of RecurDyn is 1×10^{-6} s, and the total simulation duration is 14 s. The calculation time step of EDEM is set at 30% of the RecurDyn time step and saved every 0.05 s. The grid size of the computational domain is typically twice the radius of the smallest particle. Specifically, the grid size of the coal bottom plate is 24 mm, and the total number of grids amounts to 1,050,525.

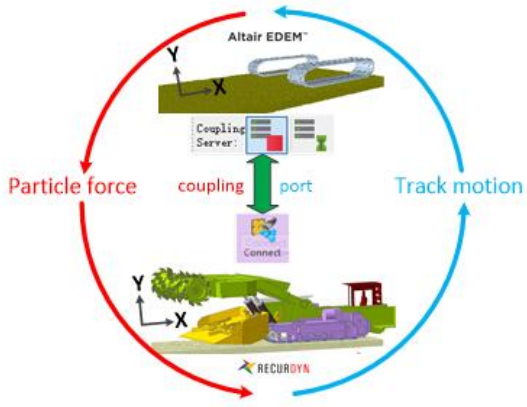

Figure 14. Bidirectional Coupling Model of Continuous Miner.

4. Analysis of simulation results of propulsion cutting conditions

The dynamic characteristics of the continuous mining machine

under the advancing cutting condition can be analyzed in detail via the two-way coupling simulation, encompassing the variations in the movement parameters of the continuous mining machine, the deformation of the bottom plate under force, and the forces exerted on the tracks.

4.1. Analysis of the motion law of the track traveling mechanism

In the result screen for RecurDyn, call the host rack centroid state. As shown in Figure 15, at 0 s, the rotational speed of the driving wheel escalates rapidly from 0 to 5 r/min, and the continuous miner enters the cutting and propulsion state. Its maximum traveling speed is 71 mm/s (4.26 m/min), the minimum is 39 mm/s (2.34 m/min), and the average traveling speed is 56 mm/s (3.36 m/min), which approximates the set speed of 3.5 m/min. The actual traveling speed undergoes periodic variations throughout cutting and advancing, the causes of the fluctuations are attributed to the polygonal effect of the track, which is induced by the sudden force when the driving wheel engages with the track plate, resulting in the non-uniformity of the movement.

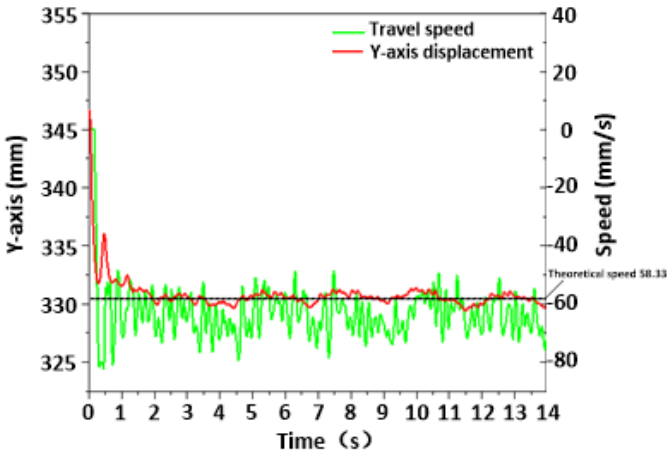

Figure 15. Centroid state of continuous mining machine.

On the other hand, the supporting section of the track exhibits a backward movement relative to the roadway floor due to the slippage between the track and the roadway floor. Hence, the actual movement speed is lower than the theoretical speed. The distance traversed by the track in the supporting section on the roadway floor is L, the horizontal deformation of the roadway floor is L_0, and the actual forward distance of the continuous miner is L-L_0. The slip rate δ of the continuous miner is:

$$\delta = \frac{L - L_0}{L} \tag{13}$$

The actual traveling speed of the track walking mechanism:

$$v_S = (1 - \delta) v_m \tag{14}$$

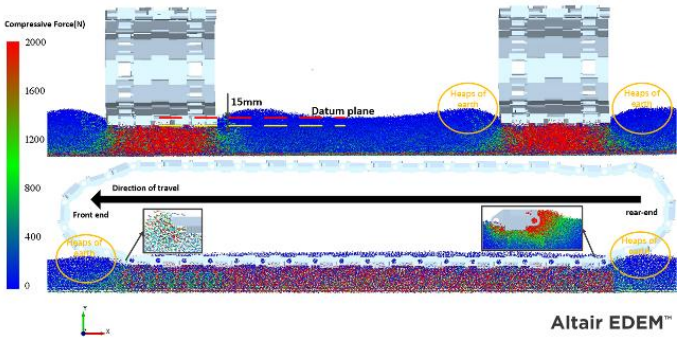

Figure 16. Ground stress deformation vector diagram.

As depicted in Figure 16, the subsidence amount gradually increases over time and stabilizes upon reaching a certain extent, the maximum deformation depth can reach 15 mm. The blue portion represents the surface area of the coal seam roadway floor, while the green portion represents the deep area. The force distribution of the coal seam roadway floor beneath the crawlers on both sides is similar. However, the pressure on the coal seam roadway floor beneath the entire crawler is unevenly distributed. The longitudinal pressure is concentrated at the middle and rear positions of the crawler, while the transverse pressure is most concentrated at the middle line of the crawler, the pressure gradually decreases away from the center line of the crawler, presenting a bell-shaped distribution. The deformation of the roadway floor is not confined to beneath the track, it rather extends to the surrounding area of the track, forming a skirt-like phenomenon (This is extremely similar to the phenomenon of wheeled vehicles [24]). Particularly, the front and rear ends of the track undergo the most intense deformation because this is where the track first contacts the undeformed roadway floor, the particles of the roadway floor near the front end bulge due to track driving. At the rear end, as the track moves backward under the action of the driving wheel, the particles bulge and form congestion.

4.2. Analysis of the contact force between the track and the driving wheel

The continuous mining machine is powered by six track plates engaged with the driving wheel. As shown in Figure 17, the contact force between each track plate and the driving wheel is

highly similar, with only a temporal phase difference. The difference in the engagement time causes this similarity due to the different relative positions of each track plate and the driving wheel. At 0 seconds after the driving wheel starts rotating, track plate 44 is the first to engage with the driving wheel. The contact force in the forward direction gradually increases when the center of mass of the track plate and that of the driving wheel are at the same height, reaching a peak of 50 KN. As the driving wheel rotates, the contact force in the X-axis direction gradually reduces until it becomes zero. The X-axis contact force remains in the same direction throughout the entire process.

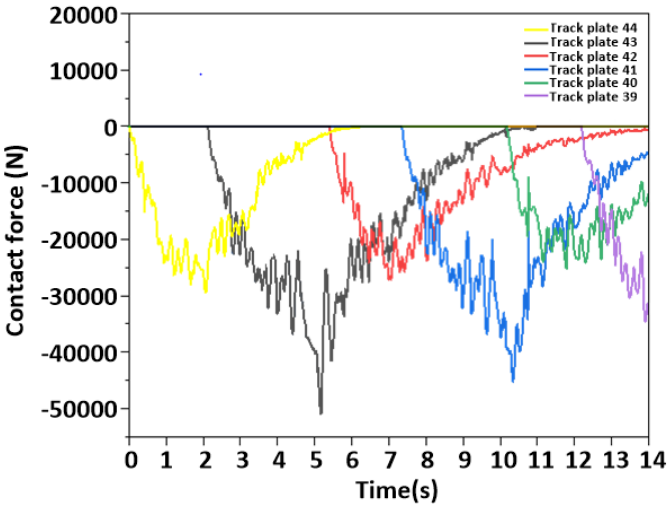

Figure 17. Track plate and driving wheel forward direction contact force.

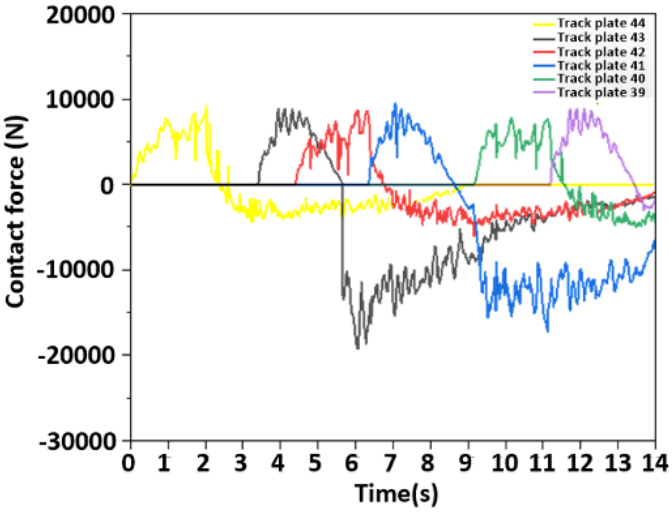

Figure 18. Contact force between track plate and driving wheel in vertical direction.

As shown in Figure 18, when the track plate moves under the driving wheel, the contact force in the Y-axis direction reaches a negative peak because the driving wheel bears part of the vertical load and acts on the track plate, averaging -20 KN. When the center of the track plate mass is at the same height as that of the driving wheel, the contact force in the Y-axis direction is reduced to zero. Subsequently, the track plate and the driving wheel continue to mesh. The contact force in the vertical direction changes from the negative in the Y-axis to the positive until the center of mass of the track plate is directly above the driving wheel, reaching a positive peak with an average of 10 kN. As the driving wheel rotates further, the contact force in the Y-axis direction gradually decreases until it reaches zero.

Since the center of mass of the track plate has almost no relative position change in the Z-direction and there is only a slight oscillation, the contact force in the Z-direction is approximately zero, as shown in Figure 19.

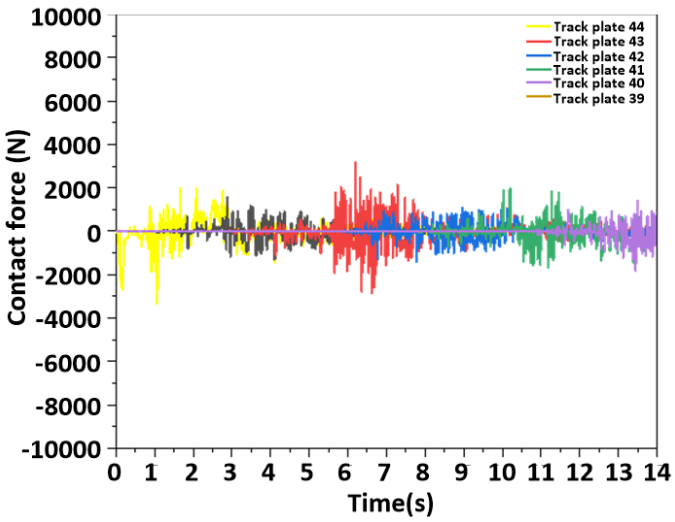

Figure 19. Track plate and drive wheel Z-axis direction contact force.

4.3. Analysis of track plate forces

As shown in Figure 20, the track plates 47, 1, 5, 9, 13, and 17 are positioned at the loose edge, and their stress is comparatively small, the track plates 21, 27, 31, 35, 39, and 43 are located at the tight edge, hence, their stress is greater. The closer a track plate is to the driving wheel, the greater the stress. This phenomenon is caused by the stress condition of the track. On the one hand, the track plate acts upon the track connected to the body part via the cantilever due to the cutting resistance and resistance moment of the cutting drum, generating a backward tilting moment. Consequently, a more pronounced force is exhibited on the rear end of the track. On the other hand,

as the driving wheel supplies power to the track, the adjacent track plates are subjected to a greater tensile force and load. Hence, the stress of track plate 43 increases, the stress of the track plate 43 is depicted in Figure 21, at 1.96 s, the node point is 57 955, the maximum equivalent stress is 758.27 MPa, and the maximum equivalent stress node is situated at the rounded corner where the track plate is in contact with the driving wheel.

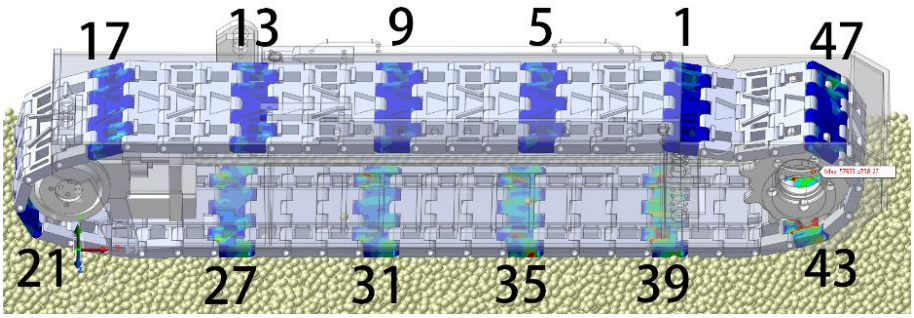

Figure 20. Side track stress cloud image.

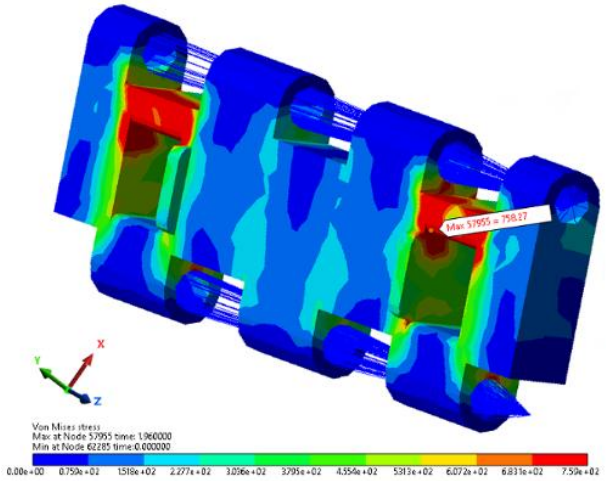

Figure 21. Track plate 43 stress nephogram.

The track plate is fabricated from 42CrMo (modulated) forging material, characterized by excellent strength and toughness. According to the simulation results, the safety coefficient of the track plate is calculated as 1.201. Although this value lies within the yield limit range of the material, its safety coefficient is relatively low. Generally, the safety coefficient is selected between 1.2 and 2.5 [20], and even higher in the case of extreme load. This result indicates that the safety coefficient needs to be enhanced, and there is considerable scope for optimizing the track plate structure. The deformation of the track plate is also very important, but the deformation can be calculated directly in the contour module in the RecurDyn software, with a maximum deformation distance of 2.78 mm.

5. Optimized design of track plate structure based on the ISIGHT platform

ISIGHT is a professional software encompassing multiple subject domains and supporting multi-objective optimization. ISIGHT mainly comprises three major modules (Figure 22): (1) DOE design module, (2) approximation agent module, and (3) optimization module.

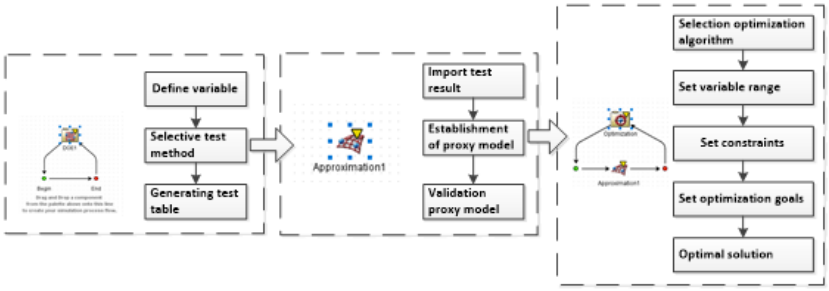

Figure 22. ISIGHT optimization flow chart.

5.1. Experimental design of DOE

(1) Selection of design variables and sampling methods

According to the simulation results and the rationality of the design, the overall size of the track plate body remains unchanged. Moreover, the structural parameters of the track plate are optimized based on the original track plate dimensions [29], the specific design variables are presented in Figure 23, and the range of values of the design variables is shown in Table 4.

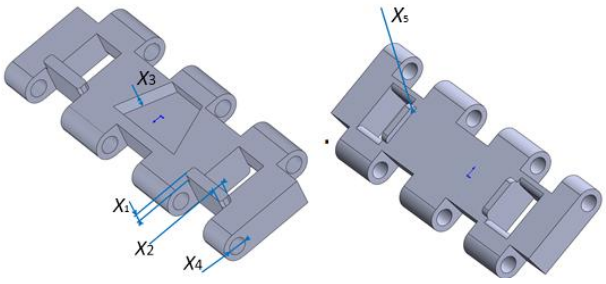

(a) Outer surface of the track plate (b) inner surface of the track plate

Figure 23. Track plate design parameters.

Table 4. Design variables and their value ranges.

Design variable	Initial value	Range of variable
Heel height X_1（mm）	14	10-40
Width of thorn X_2（mm）	18	10-30
Groove depth X_3（mm）	23	13-30
Pin hole diameter X_4（mm）	29	27-31
Rounded radius X_5（mm）	5	2.5-5.5

The sample points are reasonably and uniformly distributed in the design space, avoiding the aggregation and deviation of the sample points. Then, the influence of each design variable on the target performance is explored, improving the accuracy and reliability of the model prediction. The optimal Latin Hypercube method is selected for sampling in the ISIGHT of dassault systemes. The formula 2×(n+1)(n+2) is commonly used in the design of experiments (DOE) to estimate the minimum number of samples required by the optimal Latin Hypercube method to ensure the accuracy of the agent model, as presented in Table 5. Eighty sets of training samples are generated in the table of the range of values, where X_1-X_5 is the design variable, Y_1 is the stress value of the third section coupling simulation, and Y_2 is the quality of the track plate in the coupling model.

Table 5. Track plate design variable part selection point.

No.	X_1	X_2	X_3	X_4	X_5	Y_1 Equivalent stress（MPa）	Y_2 Quality（kg）
1	14.18	19.11	14.51	28.57	3.515	778.019	27.902
2	29.75	15.57	13	28.975	3.955	777.064	27.406
3	14.94	29.49	17.95	30.089	5.22	805.223	30.322
4	15.7	28.48	25.48	28.367	6.615	777.185	27.419
5	20.25	21.65	30	29.076	5.665	792.109	29.111
6	29.37	20.13	26.99	30.899	6.11	780.771	28.177
……	……	……	……	……	……	……	……
……	……	……	……	……	……	……	……
……	……	……	……	……	……	……	……
……	……	……	……	……	……	……	……
76	21.39	16.08	13.43	30.595	5.35	788.299	29.760
77	30.51	11.52	15.58	29.329	6.472	778.306	79.810
78	22.91	22.41	13.22	28.772	5.73	780.480	18.594
79	38.48	24.68	22.9	27.962	6.74	782.871	19.055
80	36.58	16.84	16.66	30.848	5.54	775.359	20.973

(2) Analysis of parameter sensitivity

A sensitivity analysis of the track plate's structural parameters is conducted, the Pareto plot of the response function corresponding to the optimization objective can be obtained once the ISIGHT calculation program is completed, the Pareto plot can visually analyze the percentage contribution of the five parameter variables to the objective function.

The contribution rates of the Pareto charts generated by the DOE analysis are ranked in descending order. As shown in Figure 24(a), X_2 has the greatest influence on the quality of the track plate, with a contribution of 40.546%. Parameter X_3 has the second-highest influence, with a contribution of 25.926%, followed by X_1 with a contribution value of 16.77%, X_4 with a contribution of 15.982%, and X_5 with a contribution of 0.777%. The effects of X_1 and X_2 are positive, while the effects of X_3, X_4, and X_5 are negative. A positive effect means the target value increases with the design variables, while a negative effect is the opposite. According to Figure 24(b), X_5 has the greatest influence on the maximum equivalent stress of the structure, with a contribution of 52.57%. Parameter X_4 has the second-greatest influence on the maximum equivalent stress, with a contribution of 19.555%, followed by X_1 with a contribution value of 14.41%, X_3 with a contribution value of 9.167%, and X_5 with a contribution value of 4.303%. The influence of X_2, X_4,

and X_5 is positive, while the influences of X_1 and X_3 are negative.

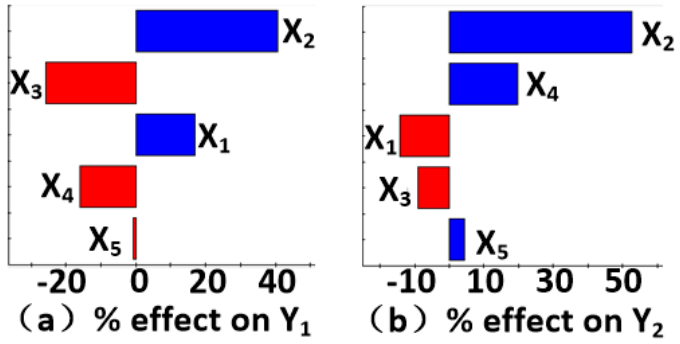

Figure 24. Pareto contribution rate of design variable to response goal.

5.2. Construction and validation of the surrogate model

The surrogate model is a method used to predict unknown points by constructing the response relationship between the independent and dependent variables using the existing data. The Kriging model [30] is an interpolation technique, and various correlation functions can be selected to construct the meta-model; thus, the model is characterized by great flexibility. In the approximation module, 80 samples collected by optimal Latin Hypercube sampling are used to construct the Kriging surrogate model. The remaining 20 samples are used to evaluate the accuracy of the surrogate model. The error analysis is performed using the fit evaluation coefficient (R-squared). The results are shown in Figure 25. The R^2 value of the maximum equivalent stress Y_1 is 0.95084, and that of the mass Y_2 is 0.93126. Since both values are greater than 0.9, the fitting effect is good.

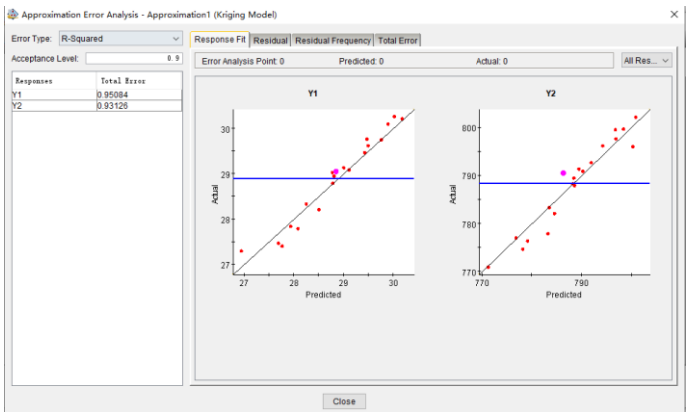

Figure 25. Error analysis of proxy model.

5.3. Multi-objective optimization based on the Kriging model

(1) optimization objectives and constraints

The tracked traveling mechanism of the continuous mining machine comprises 100 track plates, each track piece weighs 28 kg, and the mass of the track plates of the entire traveling mechanism totals 2.8t. The substantial weight has a considerable impact on the mobility of the tracked mechanism. Moreover, high requirements are placed for motor performance, transmission systems, and drive wheels. According to the simulation analysis results in section 3, the stress of the track plate is relatively high, and the safety margin is insufficient under the cutting and propelling conditions of the continuous mining machine.

The structural optimization design of the track plate is carried out without changing the kinematic parameters to address the problems of the track plate's low safety coefficient and heavy mass. The specific expressions are as follows:

$$\begin{gathered} min\ m \\ min\ \sigma(X) \\ s.t.\begin{cases} \sigma(X) < \sigma_0(X) \\ \delta(X) \le \delta_0 \\ X = (x_1, x_2, \cdots, x_5)^T \\ x_{min} \le x_i \le x_{max} (i = 1,2, \cdots 5) \end{cases} \end{gathered} \tag{15}$$

where X represents the optimization design variable, $x_{\min}$ indicates the lower limit of the design variable, and $x_{\max}$ denotes the upper limit of the design variable; m is the mass of the track plate; σ(X) is the maximum equivalent stress of the track plate; σ_0 (x) is the maximum equivalent stress of the track plate before optimization; δ(X) is the maximum static deformation of the track plate; and δ_0 is the maximum deformation of the track plate before optimization, which is 2.78 mm.

(2) genetic algorithm optimization

Genetic algorithms can solve a wide variety of problems. However, they are prone to premature convergence. Deb [31] proposed the Non-dominated Sorting Genetic Algorithm-II (NSGA-II) in 2000 to improve the shortcomings of genetic algorithms that lead to early convergence when solving optimization problems. This algorithm is a genetic algorithm based on Pareto optimality and is an improvement based on the Genetic Algorithm (GA) and a series of derived algorithms.

The improvement aspects are as follows. NSGA-II introduces a fast, non-dominated sorting algorithm, reducing the computational complexity from $O(MN^3)$ to $O(MN^2)$. Simultaneously, NSGA-II adds a congestion distance evaluation

to maintain population diversity and avoid solutions aggregation by quantifying the solutions' distribution density. Moreover, NSGA-II adopts an elitist strategy by merging the current population with the offspring and filtering them to ensure the retention of high-quality solutions and the continuous optimization of the Pareto frontier. NSGA-II can deal with the conflicts and contradictions between the objectives in the multi-objective parallel optimization problem, providing diversified solutions to meet the complex needs of practical projects [32]. For example, NSGA-II can be used in structure optimization, path planning, and resource scheduling, the specific process is shown in Figure 26.

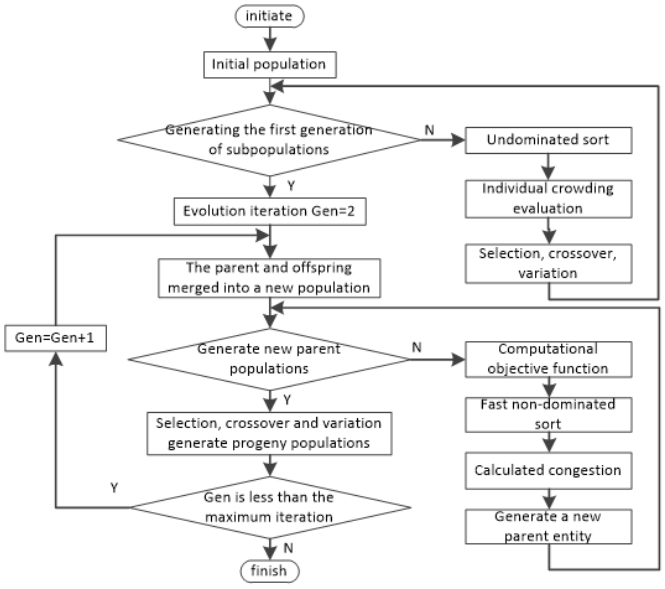

Figure 26. Flowchart of NSGA-II algorithm.

The optimization algorithm and related parameters are set in the optimization module, the optimization algorithm adopts the second-generation NSGA-II. The population size, the number of evolutionary generations, and the crossover probability of the algorithm are set to 20, 200, and 0.9, respectively. Finally, the output response variable is minimized for optimal search.

Before running the model, the corresponding components can be selected, and monitoring can be added on the chart property page to observe the changes in the design variables and the objective function in real time during the running process. Several target iterations are conducted to obtain the solution set of the Pareto frontier, as shown in Figure 27. The objective function's value is higher in the initial stage (with greater randomness). With iterations, the value of the objective function gradually decreases and stabilizes, indicating that the optimization algorithm gradually converges. The sample points are stabilized after 700 iterations. In the figure, the blue points indicate the optimal solution set, and the green points indicate the optimal point.

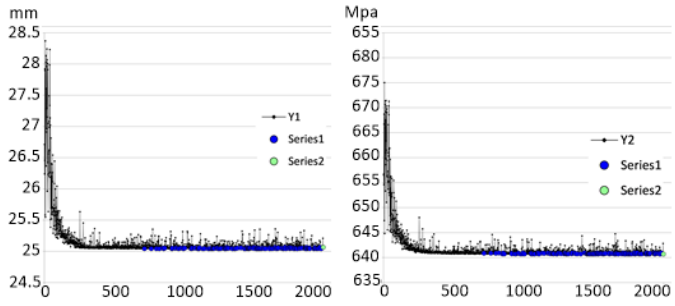

Figure 27. Pareto frontier solution set.

The green dot in Figure 28 was chosen as the optimal solution for the target design variables, the comparative results before and after optimization are presented in Table 6.

Table 6. Design variable values and target values before and after optimization.

	X_1	X_2	X_3	X_4	X_5	Y_1	Y_2
Original value	14	18	23	29	10	28kg	758.27 MPa
Optimization value	19.615	12.998	28.423	29.638	8.868	25.42 kg	642.52 MPa

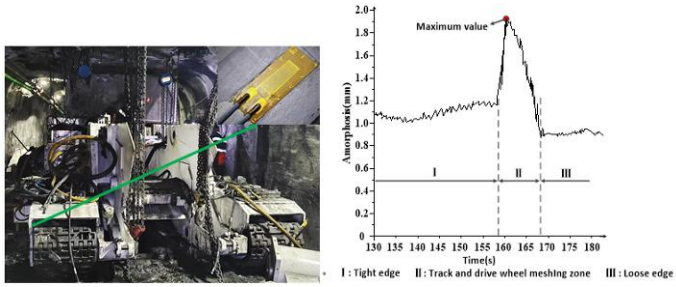

Figure 28. Industrial test.

The optimized stress value amounts to 642.52 MPa. The stress value is diminished to 70% of the yield strength of the material, and the safety coefficient is augmented to 1.43, signifying that the optimization outcome is rational [33]. The optimized track was modeled and assembled, and its performance was verified using the bidirectional coupling simulation of RecurDyn and EDEM. The simulated stress value was 662.43 MPa, with an error rate of 1.95% compared to the optimized value. The optimized track weighed 25 kg, representing a 10% weight reduction. The overall weight reduction of the continuous miner was 258 kg. The optimized maximum deformation was 1.98 mm. Since the stress of the track of the continuous mining machine cannot be directly

measured, the deformation amount is selected as one of the experimental verification methods, which indirectly indicates the reliability of the optimized track plate. For the test, strain gauges were installed at critical locations on the optimized track plates, such as contact surfaces and gear contact points, to monitor the strain during operation. When the continuous miner was operated at an advanced cutting speed of 3.5 m/min and a drum rotation speed of 51 r/min, the measured maximum deformation value was 1.96 mm. This value is reduced compared to the pre-optimization value. The experimental data agree with the optimization results, meeting the theoretical expectations. The performance of the optimized track plates was monitored after they were put into service (Figure 28). The track plates performed well during operation, with reliable performance, no failures were recorded during 7,500 hours of service in a 4.3 m-thick coal seam, indicating a significant improvement in the performance of the optimized track plates.

6. Conclusions

Based on EDEM software and RecurDyn software, the bidirectional coupling model of cutting and advancing conditions of continuous mining machine is constructed, and the change of track motion parameters, the stress deformation of bottom plate and the stress of track are studied. Based on bidirectional coupling simulation combined with Kriging agent model and genetic algorithm, determined the optimal design scheme of track plate structural parameters. The main contributions are as follows:

(1) Grounded on the physical and mechanical properties of the coal and rock mass and the coal-breaking theory of the pick-type cutter, compiled a load calculation program for the continuous miner's drum using MATLAB, obtaining the three-way force and moment curves of the drum load.

(2) The two-way coupling simulation model of RecurDyn-EDEM was erected. The load was predominantly distributed on the tight edge of the track (The side of the track that comes into contact with the ground), increasing as the distance to the driving wheel was reduced. The stress distribution information of the track plate was attained, and the maximum equivalent stress node was situated at the rounded corner where the track plate contacted the driving wheel.

(3) According to the variable sensitivity analysis of the DOE module of the ISIGHT platform and the Pareto chart contribution rate, the track spur width X_2 (the width of the ground-contacting protrusions) exerted the most significant positive influence on the track plate mass. In contrast, the slot depth X_3 (he depth of the groove in the middle of the track plate) had the most substantial negative influence. The track spur width X_2 had the greatest positive impact on the maximum equivalent stress, and the track spur height X_1 (The height of the raised part on the ground) had the most pronounced negative influence.

(4) The track spur height, track spur width, groove depth, pinhole diameter, and the radius of the contact rounded corner between the track and the driving wheel were selected as the design variables. the NSGA-II algorithm was utilized for optimization via the ISIGHT platform's optimization module. The optimized stress value was 642.52 MPa, the simulated value was 662.43 MPa, the safety coefficient was elevated to 1.43, corresponding to 70% of 42CrMo's yield strength (910 MPa), meeting the safety margin requirement of 1.2–2.5 for mining machinery. the optimized mass was 25.42 kg (a 9.2% reduction), the weight of the entire machine was reduced by 258 kg, and the optimized maximum deformation was 1.98 mm. The industrial test of the optimized track plate shows that there is no failures were recorded during 7,500 hours of service in a 3.5 m-thick coal seam, and the performance of the optimized track plate is obviously improved.

Funding

This work was part of a research project on "Research on the dynamic characteristics of thin coal seam containing hard-tubercular broken by the spiral drum of the coal shearer" funded by Liaoning Provincial Department of Education, China (grant no. LJ212410147026) and "Research on mechanism of collaborative coal and rock crushing with pick Group and optimization design of spatial position parameters based on factor space method" funded by Science and Technology Department of Ningxia (grant no.

2024BEH04164).

References

1. Zhao L J, Yang S J, Zhang H N , Han L G. Fatigue life prediction of shearer rocker arm housing based on DEM-MFBD bidirectional coupling technology. Coal Science and Technology 2023; 51(S2): 252–258. DOI: 10.13199/j.cnki.cst.2022-1908.
2. Bekker M G. Theory of Land Locomotion: The Mechanics of Vehicle Mobility. Ann Arbor: University of Michigan Press, 1956. DOI: 10.3998/mpub.9690401.
3. Xu W, Gao K, Wang S, Jiang K, Jiang W, Dong G. Cutting load analysis and optimization methods of the bauxite shearers. Eksploatacja i Niezawodność – Maintenance and Reliability 2025; 27(3): 201464. DOI: 10.17531/ein/201464.
4. Wan L, Jiang K, Zeng Q, Gao K. Dynamic response and reliability analysis of shearer drum cutting performance in coal mining process. Eksploatacja i Niezawodność – Maintenance and Reliability 2022; 24(1): 123–129. DOI: 10.17531/ein.2022.1.14.
5. Han S R, Huh K S, Bae D S, Choi J H. Development of a multibody dynamics simulation tool for tracked vehicles part I: efficient contact and nonlinear dynamic modeling. JSME International Journal Series C, Mechanical Systems, Machine Elements and Manufacturing 2003; 46(2): 540–549. DOI: 10.1299/jsmec.46.540.
6. Liu Z S, Lu C, Wang Y Y, Lee H P, Koh Y K, Lee K S. Prediction of noise inside tracked vehicles. Applied Acoustics 2006; 67(1): 74–91. DOI: 10.1016/j.apacoust.2005.05.003.
7. Zhu X G, Gu L, Yang C B, Gong Y J. Strength analysis of track structure based on finite element method. Manufacturing Automation 2015; 37(1): 44–46.
8. Lu T, Kang Y B, Zhao Y. Analysis and calculation of track plate for continuous miner travel unit. Coal Mine Machinery, 2013, 34(3): 37-38. DOI: 10.13436/j.mkjx.2013.03.057.
9. Zhang H, Zang X P, Shi T. Dynamic characteristics and fatigue life analysis of the track travelling mechanism of continuous mining machine. Coal Science and Technology 2016; 44(11): 110–115. DOI: 10.13199/j.cnki.cst.2016.11.021.
10. Shi JP. Force analysis of driving wheel of ML360 continuous shearer. Mech Eng Autom 2018; (3): 202–203.
11. Wei KF. Research on steering resistance of tracked vehicle on soft ground based on DEM-MBD two-way coupling [dissertation]. Changchun, Jilin University: 2020.
12. Zhang ZH. Research on dynamic load identification method of track driving system [dissertation]. Taiyuan, Taiyuan University of Science and Technology: 2021.
13. Yang SS. Stress analysis and improvement of key parts of roadheader traveling mechanism. Enterp Technol Dev 2023; (5): 83–86.
14. Živković P, Milutinović M, Tica M, Trifković S, Čamagić I. Reliability Evaluation of Transmission Planetary Gears “bottom-up” approach. Eksploatacja i Niezawodność – Maintenance and Reliability 2023; 25(1): 2. DOI: 10.17531/ein.2023.1.2.
15. Gao H, Wang Y, Xu J, Qin H. Fatigue strength reliability assessment of turbofan blades subjected to intake disturbances based on the improved kriging model. Eksploatacja i Niezawodność – Maintenance and Reliability 2025; 27(2): 194175. DOI: 10.17531/ein/194175.
16. Lao J, Wang X, Zhang M, Chen Z, Guo J. Analysis and Improvement of Coal-loading Performance and Reliability of Thin Seam Coal Shearer Drums. Eksploatacja i Niezawodność – Maintenance and Reliability 2025; 27(2): 194674. DOI: 10.17531/ein/194674.
17. Ling JX. Optimal design of track plate of EBZ-135 cantilever type roadheader [dissertation]. Taiyuan, Taiyuan University of Technology: 2010.
18. Zhang L, Wang X C, Wei H L, Wang M G. Control strategy of excavator track driving mechanism based on fuzzy GA algorithm. Mechanical Design and Manufacturing 2014; (10): 220–223. DOI: 10.19356/j.cnki.1001-3997.2014.10.066.
19. Fei Y, Li Y Y, Ye X S. Track parameter optimization of TBM based on driving theory. Mining & Processing Equipment 2015; 43(2): 23–26. DOI: 10.16816/j.cnki.ksjx.2015.02.007.
20. Qin L Y. Analysis of track vehicle performance and optimization of track plate structure parameters [Dissertation]. Xiangtan: Hunan University of Science and Technology 2020. DOI: 10.27738/d.cnki.ghnkd.2020.000282.
21. Si L P. Research on optimization and improvement of track plate structure of mining TBM. Coal and Chemical Industry 2020; 43(5): 89–91. DOI: 10.19286/j.cnki.cci.2020.05.025.
22. Zheng XJ, Wang ZB. Optimization of contact parameters between crawler crane support wheel and crawler plate structure. Constr Mach 2022; (3): 71–75.

23. Yuan SH. Analysis of contact mechanical characteristics of track of anchor digger based on DEM-MBD coupling [dissertation]. Fuxin, Liaoning Technical University: 2022.
24. Wang X, Lu Y, Cheng P, Wen M, Zhang Y. Coupled discrete element-particle analysis of single-wheel and four-wheel off-road vehicle on soft ground. Soil Dynamics and Earthquake Engineering 2025; 199: 109639. DOI: 10.1016/j.soildyn.2025.109639.
25. Liang J. Dynamic analysis and fatigue reliability study of running part of continuous shearer [dissertation]. Taiyuan, Taiyuan University of Technology: 2010.
26. Zhang YP. Study on the influence of kinematics parameters and structure parameters of continuous mining drum on cutting performance [dissertation]. Fuxin, Liaoning Technical University: 2024.
27. Ma J G. Research on the development status of short-wall mechanized mining of continuous shearer. Coal Science and Technology 2020; 48(9): 180–188. DOI: 10.13199/j.cnki.cst.2020.09.023.
28. Chang S. Research on the dynamics of track traveling mechanism of tunnel boring machine [dissertation]. Fuxin, Liaoning Technical University: 2012.
29. Yang C B, Gu L, Li Q. Finite element simulation of track shoe and ground adhesion. Applied Mechanics and Materials 2014; 644-650: 402–405. DOI: 10.4028/www.scientific.net/AMM.644-650.402.
30. Ren M, Wang Z F, Xu H, Wang Y. Optimization of fuzzy PID control in reactor based on genetic algorithm. Automation Technology and Application 2025; 44(6): 22–27. DOI: 10.20033/j.1003-7241.(2025)06-0022-06.
31. Deb K, Agrawal S, Pratap A, Meyarivan T. A fast elitist non-dominated sorting genetic algorithm for multi-objective optimization: NSGA-II. In: Schoenauer M, et al., eds. Parallel Problem Solving from Nature – PPSN VI. Lecture Notes in Computer Science, vol 1917. Berlin: Springer, 2000; 849–858. DOI: 10.1007/3-540-45356-3_83.
32. Xu L. Research and application of multi-objective optimization problem based on genetic algorithm [dissertation]. Changsha, Central South University: 2007.
33. Rozvany G I N. A critical review of established methods of structural topology optimization. Structural and Multidisciplinary Optimization 2009; 37(3): 217–237. DOI: 10.1007/s00158-007-0217-0.